EEET ECOLOGICAL ENGINEERING & ENVIRONMENTAL TECHNOLOGY

Ecological Engineering & Environmental Technology, 2026, 27(9), 361–378
https://doi.org/10.12912/27197050/226530
ISSN 2719–7050, License CC-BY 4.0

Received: 2026.07.13
Accepted: 2026.08.03
Published: 2026.08.15

Temporal resolution requirements for event-oriented indoor air quality monitoring: Peak attenuation, missed events, and event-ranking reversals

Carlos Jamil Bastidas Sánchez[1*]

[1] Facultad Ciencias de la Ingeniería, Universidad Estatal de Milagro, Milagro, Ecuador
* Corresponding author's e-mail: cbastidass@unemi.edu.ec

ABSTRACT

Indoor air-quality networks are often configured around storage, power, or communication constraints, although the reporting interval can determine whether short events are detected and which event is judged most important. This study quantified that effect without introducing between-instrument confounding. Two co-located technical-replicate units from one EDIAQI low-cost-sensor provider were analyzed within each documented event rather than counted as independent environmental observations. Native approximately 5-s data for $PM_{2.5}$, CO_2, and the sensor-reported total volatile organic compound (TVOC) response were aligned with 26 documented indoor, activity, emission, and ventilation events. Each native series was degraded within sensor to 30-s, 1-, 5-, 10-, 15-, and 30-min reporting by both non-overlapping block averaging and instantaneous sampling. Every possible 5-s phase offset was evaluated. Outcomes were baseline-relative peak retention, net-excursion area-under-the-curve (AUC) retention, event detection using resolution-specific quiet-period thresholds, and event-ranking stability. Uncertainty was estimated by 2,000 event-level bootstrap resamples after reducing phase offsets and technical units within event. At 5-min block averaging, median peak retention was 0.771 (95% bootstrap interval: 0.598–0.895) for $PM_{2.5}$, 0.987 (0.967–0.996) for CO_2, and 0.982 (0.914–0.992) for TVOC response, whereas median net-AUC retention remained 0.998, 1.001, and 0.998, respectively. The native $PM_{2.5}$ top-ranked event (oil diffuser) was replaced by an exercise/open-door event in both units for all 60 five-minute phase offsets. At 10 min, mean missed-event probability was 0.434 for $PM_{2.5}$, 0.104 for CO_2, and 0.146 for TVOC response. Instantaneous sampling was more phase-sensitive than block averaging. These results show that temporal resolution should be specified from the monitoring decision: intervals that are adequate for integrated event burden can be inadequate for peaks, alarms, or event prioritization. The numerical limits are empirical for the monitored environment and should be transferred only after considering event time scale and sensor response.

Keywords: indoor air quality, temporal aggregation, low-cost sensors, particulate matter, carbon dioxide, total volatile organic compound response, event detection, monitoring design.

INTRODUCTION

Indoor pollutant concentrations can change over seconds to minutes because of cooking, combustion, cleaning, human activity, door opening, and the transport of outdoor air (Cowell et al., 2023; Ilacqua et al., 2022). Residential studies based on continuous monitoring consistently show that episodic indoor sources can create sharp concentration excursions whose magnitude and timing are poorly represented by longer-term summaries (Ferro et al., 2022; Mousavi and Wu, 2021). Event-resolved and high-spatiotemporal-resolution analyses confirm that these transient indoor contributions remain distinct even in large residential datasets (Byrne et al., 2023; Lunderberg et al., 2023). The environmental meaning of a reported value therefore depends not only on the sensor and pollutant, but also on how frequently the value is produced and whether it represents an interval average or a momentary observation (Bean, 2021; Bulot et al., 2023).

Low-cost monitors make dense, multipollutant indoor monitoring feasible, but their outputs are not equally interpretable across variables (Ródenas García et al., 2022; Sá et al., 2022). Controlled evaluations show that optical PM sensors are useful for relative temporal dynamics while remaining sensitive to aerosol properties and humidity, whereas CO_2 channels tend to be more stable for event tracking (Demanega et al., 2021; Manu and Rysanek, 2024). Multipollutant system studies reinforce the need for channel-specific validation (Chojer et al., 2024; Corona et al., 2024), and metal-oxide VOC outputs can show device-dependent magnitude, baseline, selectivity, cross-sensitivity, and response or recovery time (Isaac et al., 2022; Papale et al., 2023). Consequently, the present analysis does not treat the selected variables as interchangeable absolute concentrations. $PM_{2.5}$ and CO_2 are analyzed as within-sensor, event-relative measurements, and the TVOC channel is explicitly described as a sensor-reported response rather than a chemically resolved TVOC concentration (Baldelli, 2021; Papale et al., 2023).

The ability to report at high frequency is often presented as an intrinsic advantage of low-cost sensing (Sá et al., 2022; Zimmerman, 2022). In practice, deployed networks routinely transmit or store 1-, 5-, 10-, or 30-min values to reduce power, storage, and communication demand (Barros et al., 2023; Wall et al., 2021). Where high-frequency noise dominates, aggregation can improve precision or agreement, and coarser averaging is appropriate for some regulatory or exposure summaries (Bean, 2021; Chacón-Mateos et al., 2025). The same operation, however, suppresses transient maxima and can merge adjacent episodes, so apparent monitor performance shifts with the averaging period and the processing choices adopted (Bulot et al., 2023; Frischmon et al., 2025). Temporal aggregation is therefore neither uniformly beneficial nor uniformly harmful: its adequacy depends on the decision the data must support.

This distinction is especially important for the contrast between cumulative burden and short-term decision outcomes. A correctly weighted block mean can approximately preserve the integral of a signal over a fixed event window even while lowering its maximum. Thus, a reporting interval may be acceptable for event-integrated exposure or burden but fail for threshold exceedance, alarm triggering, or identification of the event with the largest peak (Bean, 2021; Bulot et al., 2023). Merely observing that averaging lowers a peak would be arithmetically unsurprising; recent sensor evaluations show that average-fit metrics can conceal errors at transient maxima and that conclusions change with averaging time (Bean, 2021; Frischmon et al., 2025). The scientifically and operationally relevant questions are how much is lost for different pollutant-response regimes, at what interval a documented event is no longer reliably detected, and whether aggregation changes the event priority that a monitoring program would communicate (Bulot et al., 2023; Jones et al., 2024).

Existing indoor low-cost-sensor work has primarily emphasized instrument performance and calibration (Sá et al., 2022; Tryner et al., 2021), long-term concentration patterns and indoor/outdoor relationships (Lunderberg et al., 2023; Wallace and Zhao, 2023), or source characterization (Bousiotis et al., 2023; Rathbone et al., 2025). Temporal-resolution effects have been considered more often through outdoor, mobile, or calibration agreement statistics than through event-aware, multipollutant decision outcomes (Bean, 2021; Whitehill et al., 2024). The extension to an indoor setting with known event timing, two co-located units, alternative reporting protocols, all phase offsets, and simultaneous evaluation of peak, AUC, detection, and ranking has not been resolved by that literature (deSouza et al., 2023; Levy Zamora et al., 2023). This is a narrow methodological gap with a direct engineering consequence: a network designer needs an interval that is fit for the intended inference, not simply the longest interval that reduces data volume (Barros et al., 2023; Wall et al., 2021).

The open EDIAQI dataset offers an unusually strong design for this question. Its Data Descriptor documents household-like emissions, human activities, and ventilation events in an experimental room, with synchronized low-cost and reference measurements (Lovrić et al., 2025). Rather than infer an unobserved process from sparse samples, the present study treats the native high-frequency record as an operational reference, degrades it deliberately, and measures the resulting loss against the known native series, consistent with reproducible high-resolution sensor-evaluation practice (Bulot et al., 2023; Diez et al., 2024). Comparisons are made within each sensor. The two co-located units are then used to require replication: a ranking reversal is classified as robust only when both units agree on the native ordering and both agree on the reversed degraded ordering. The use of replicate-device disagreement as an empirical quality signal is supported by large co-location and twin-channel studies (deSouza et al., 2023; Manu and Rysanek, 2024).

The objective was to quantify temporal-resolution requirements for event-oriented monitoring of $PM_{2.5}$, CO_2, and sensor-reported TVOC response within the monitored EDIAQI environment. Two reporting mechanisms were distinguished – interval block means and instantaneous samples – because the distinction is consequential for transient-event capture (Bean, 2021; Chacón-Mateos et al., 2025). We hypothesized that (i) block averaging would preserve event-integrated net AUC more effectively than peak magnitude; (ii) $PM_{2.5}$ would be more resolution-sensitive than the more sustained CO_2 response; (iii) instantaneous sampling would show greater phase dependence than block averaging; and (iv) sufficiently coarse reporting would produce twin-confirmed ranking reversals. A baseline-corrected half-height width was used as the primary nonparametric event time scale, while exponential decay constants were retained only as a secondary physical interpretation for eligible clean decays (Glenn et al., 2023; Jones et al., 2024). The study does not propose universal indoor sampling limits. It estimates decision-specific limits for one monitored environment and provides a reproducible procedure that can be applied to other high-frequency event datasets (Bulot et al., 2023; Frischmon et al., 2025) (Figure 1).

MATERIALS AND METHODS

Data source, version, and analytical scope

The analysis used the latest EDIAQI Zenodo version available when the workflow was executed: version DOI 10.5281/zenodo.17151843, licensed CC BY 4.0. The associated Data Descriptor explains the experimental room, instruments, household-like activities, and timestamped events (Lovrić et al., 2025). To make version dependence explicit, the source archive checksum was MD5 0cb0075b823953a6d949ae2c70430aa3 and the event JSON checksum was dc58f4e626cb9c666fb-63578f9a4934f; versioned files and checksums follow current recommendations for auditable sensor datasets (Diez et al., 2024; Fissore et al., 2024).

The primary analysis was restricted to Provider 4 because it contained two co-located units with the highest nominal reporting frequency among the multipollutant providers. This restriction prevents sensor technology, provider, calibration, and coverage from being confounded with reporting interval, a problem emphasized in co-location and multi-device evaluations (deSouza et al., 2023; Manu & Rysanek, 2024). The downloaded Provider 4 CSV contained 344,733 rows and 31 columns: one timestamp and 30 measurement columns, corresponding to 15 variables per unit. The exact file contained fewer rows than the count stated in the Data Descriptor for an earlier repository distribution (Lovrić et al., 2025); all results here are tied to the checked archive and manifest rather than to the article's row count (Diez et al., 2024; Fissore et al., 2024).

Three responses were prespecified as the core: $PM_{2.5}$, CO_2, and the sensor-reported TVOC response. $PM_{2.5}$ was used for within-sensor relative dynamics rather than absolute gravimetric accuracy, and CO_2 was retained as the most defensible gas-like occupancy/combustion response (Manu & Rysanek, 2024; Tryner et al., 2021). The Provider 4 TVOC field was

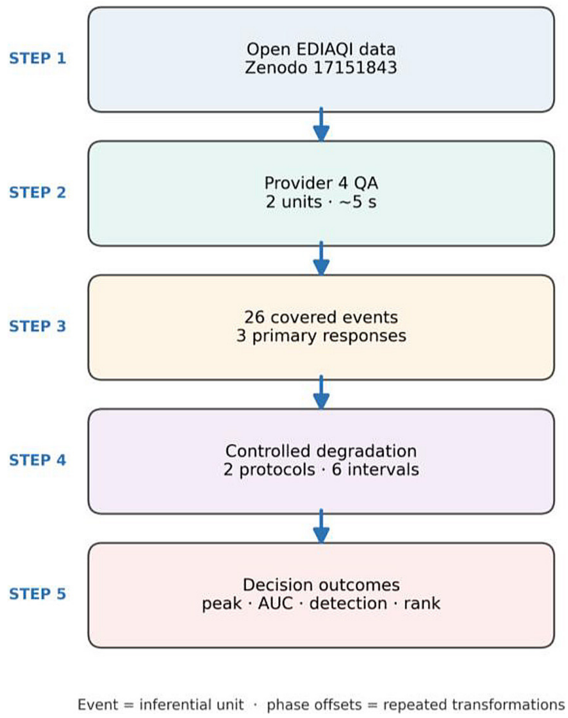

Figure 1. Reproducible analysis workflow. Provider 4 was used for the primary controlled degradation so that reporting interval changed within sensor. The documented event, not the phase offset, was the inferential unit

analyzed as a device response in its distributed units and was never interpreted as a speciated or instrument-independent concentration (Isaac et al., 2022; Papale et al., 2023). PM_{10} and electrochemical gas channels were excluded from the core because coarse-particle extrapolation, cross-sensitivity, environmental dependence, and sensor response time could dominate the apparent temporal behavior (Chacón-Mateos et al., 2025; Sá et al., 2022). Those channels can be examined in a separate robustness study but do not support the central design claim (Corona et al., 2024; Fissore et al., 2024).

Timestamp processing and quality audit

Timestamps were parsed as the Zagreb local times distributed by the repository; no UTC conversion was imposed. Duplicate timestamps (n = 1.008) were collapsed by the within-timestamp median. Because observations exhibited minor clock displacement around the nominal 5-s cadence, values were assigned to fixed 5-s bins by timestamp and collapsed by the median. No interpolation, smoothing, calibration model, or value-based outlier removal was applied. This conservative processing follows the broader recommendation that sensor-network QA preserve an auditable raw-to-analysis chain and avoid transformations that are not required by the stated objective (Bean, 2021; Giordano et al., 2021).

After duplicate collapse there were 343,725 unique timestamps. The fixed grid comprised 343,336 time bins from 11 October 2024 13:30:59 to 31 October 2024 10:22:12, with a median native interval of 5 s, one gap longer than 10 s (maximum 101 s), and 488 grid rows with at least one missing selected value. The complete audit is reported in Supplementary Table S1 and the machine-readable run manifest; the source context is documented in the EDIAQI Data Descriptor (Lovrić et al., 2025), while the completeness and provenance checks follow published sensor-network QA practice (Diez et al., 2024; Levy Zamora et al., 2023).

The repository's event JSON yielded 34 timestamped event occurrences. Provider 4 fully covered 26 events, comprising 17 emissions, six activities, and three ventilation events. Event duration ranged from 5 to 92 min (median 22 min). Only fully covered events were included; no event was selected on the basis of pollutant magnitude. The event list and exclusion reasons are retained in the analysis workbook and can be checked against the published experimental description (Lovrić et al., 2025); retaining the complete event inventory avoids magnitude-based selection of conspicuous peaks (Frischmon et al., 2025; Jones et al., 2024) (Table 1).

Event baseline, native outcomes, and characteristic width

For event e, sensor unit u, and pollutant response p, the native baseline b(e,u,p) was the median of available 5-s values during the 15 min immediately before the documented event start. Baseline-relative event excursions are commonly used to separate episodic indoor signals from the local background (Jones et al., 2024; Rathbone et al., 2025). If x(t) denotes the native series, the excursion was.

$$y_{e,u,p}(t) = x_{u,p}(t) - b_{e,u,p} \tag{1}$$

Table 1. Dataset and event-inclusion audit

Audit item	Observed value
Source version	Zenodo 10.5281/zenodo.17151843
Raw Provider 4 file	344,733 rows; 31 columns
Unique timestamps	343,725
Regular 5-s grid	343,336 rows
Duplicate timestamps collapsed	1.008
Rows with any selected-value missingness	488 (0.14%)
Timestamp coverage	2024-10-11 13:30:59 to 2024-10-31 10:22:12
Events in current JSON / fully covered	34 / 26
Included event duration	5–92 min; median 22 min
Quiet pool	320.47 h

Note: Author's audit of the versioned EDIAQI archive and current event JSON.

In the equation y is the baseline-relative excursion, x is the native sensor response, b is the 15-min pre-event median, and subscripts e, u, and p identify event, sensor unit, and pollutant response. The native peak magnitude was the largest absolute baseline-relative excursion within the documented start–end interval, because high-percentile and peak behavior can be hidden by average-fit metrics (Bean, 2021; Frischmon et al., 2025):

$$P_{e,u,p}^{\text{native}} = \max_{t \in e} \left| y_{e,u,p}(t) \right| \tag{2}$$

where: P^{native} is the native peak magnitude, t indexes 5-s timestamps, and $|y|$ permits either an upward or a downward event excursion.

Absolute excursion permits both increases and decreases, which is necessary for ventilation events and gas dilution. The sign of the largest excursion was retained separately. Event-integrated quantities provide a complementary outcome to short maxima in time-resolved indoor analyses (Bulot et al., 2023; Lunderberg et al., 2023). The primary cumulative outcome was the net-excursion AUC over the documented event interval,

$$Q_{e,u,p}^{\text{native}} = \sum_i y_{e,u,p}(t_i)\, \delta t, \qquad \delta t = 5\,\text{s} \tag{3}$$

where: Q^{native} is the signed net-excursion AUC, i indexes observations inside the documented event window, and δt is the native 5-s step.

Absolute and positive-only AUCs were calculated as sensitivity outcomes. The main AUC result uses the net excursion because exact block integration should preserve signed burden when event limits and baseline are held constant; reporting both peak and integrated metrics is consistent with the need to distinguish transient maxima from cumulative signal burden (Bulot et al., 2023; Frischmon et al., 2025).

A baseline-corrected half-height width w was the primary event time scale. Starting from the largest absolute excursion, the algorithm searched left and right for the first crossing below 50% of that peak in a window extending from 15 min before the event to 60 min after it. The post-event limit was truncated at the next documented event. Widths without both crossings were explicitly labeled left- or right-censored, not imputed. As a secondary physical analysis, an exponential decay constant τ_e was estimated on the signed post-peak branch using values between 20% and 90% of the peak. Fits required at least 20 observations, a negative log-linear slope, and R^2 at least 0.80. This restriction prevented a decay model from being forced onto source-dominated, multi-peak, or poorly observed events; comparable event-resolved indoor analyses likewise restrict first-order loss estimates to well-behaved decays (Jones et al., 2024; Lunderberg et al., 2023).

Controlled temporal degradation

The same native series from each Provider 4 unit was transformed to reporting intervals Δ of 30 s, 1 min, 5 min, 10 min, 15 min, and 30 min. Two reporting protocols were evaluated, following evidence that aggregation time and reporting mode can change apparent sensor performance and short-event capture (Bean, 2021; Bulot et al., 2023).

For block averaging, the reported value for block k and phase φ was:

$$\bar{x}^{(\Delta,\phi)}(k) = \frac{1}{n_k} \sum_{t_i \in B_k(\Delta,\phi)} x(t_i) \tag{4}$$

where: $\bar{x}$ is the block-reported value, Δ is the reporting interval, φ is its clock-phase offset, k is the block index, B_k is the set of native observations in that block, and n_k is their count.

Event AUC was overlap-weighted when a block crossed an event boundary. Consequently, a block contributed only the duration that overlapped the documented event. For instantaneous sampling, one observation was selected every Δ at the corresponding phase φ. When at least one sample occurred inside an event, event AUC was estimated as the mean sampled excursion multiplied by event duration; when no in-event sample occurred, the operational excursion was zero. Keeping block means and momentary samples separate avoids conflating two reporting mechanisms with different statistical behavior (Bean, 2021; Zimmerman, 2022).

All possible 5-s phase offsets were analyzed. Thus, an interval of Δ seconds had Δ/5 phase offsets: six at 30 s, 12 at 1 min, 60 at 5 min, and 360 at 30 min. These offsets are repeated transformations of the same observed event and were not counted as independent experiments. Metrics were first reduced across phase within each event and unit; event-level values were then summarized across events. This complete-phase design prevents an arbitrary clock alignment from determining the reported performance (Bean, 2021; Bulot et al., 2023).

Peak and AUC retention were defined relative to the native metrics:

$$R^{P}_{e,u,p}(\Delta,\phi) = \frac{P^{\text{degraded}}_{e,u,p}(\Delta,\phi)}{P^{\text{native}}_{e,u,p}} \tag{5}$$

$$R^{Q}_{e,u,p}(\Delta,\phi) = \frac{Q^{\text{degraded}}_{e,u,p}(\Delta,\phi)}{Q^{\text{native}}_{e,u,p}} \tag{6}$$

The peak- and AUC-retention ratios are dimensionless; the numerator is the degraded peak or AUC at interval Δ and phase φ, and the denominator is the corresponding native metric. A value of 1 indicates exact retention. Retention can exceed one when a coarse block mixes part of an adjacent excursion into the event boundary or when the signed native AUC is close to zero. Such values were retained as diagnostic evidence rather than truncated. Median retention across events was therefore preferred to a mean, consistent with the need to inspect aggregation effects beyond a single global agreement statistic (Bean, 2021; Frischmon et al., 2025) (Figure 2).

Resolution-specific event detection

An operational quiet pool was constructed before threshold estimation. All periods from 30 min before to 60 min after every documented event were excluded. Remaining rows were required to have zero recorded people and zero motion, and periods within ±5 min of every door-state update were excluded. The resulting quiet pool contained 230,738 five-second rows, equivalent to 320.47 h; event, occupancy, motion, and door metadata originated from the EDIAQI archive (Lovrić et al., 2025). Resolution-matched background characterization is important because noise and apparent precision change with aggregation time (Bean, 2021; Bulot et al., 2023).

Detection thresholds were recomputed after every combination of pollutant, unit, interval, protocol, and phase. The primary threshold was the 99th percentile of the absolute successive differences in the corresponding degraded quiet series, an operational approach chosen to preserve

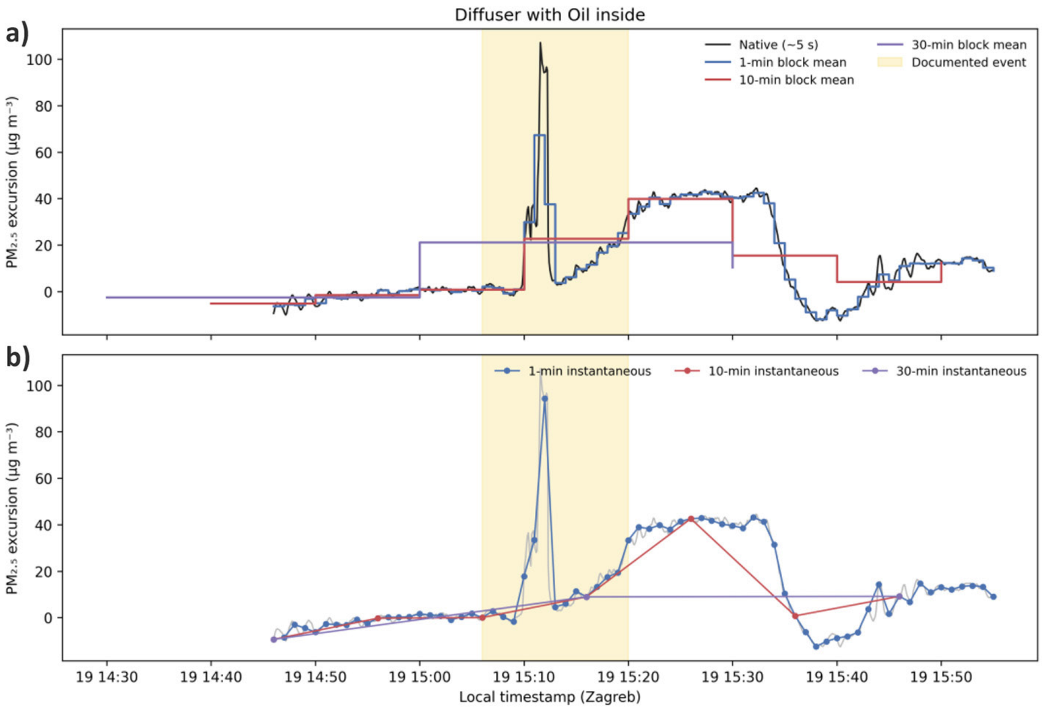

Figure 2. Example of $PM_{2.5}$ response degradation during the "diffuser with oil inside" event: a) non-overlapping block means and b) instantaneous reporting. The yellow band indicates the documented event window. A single fixed phase offset was applied to all intervals for visualization. All possible 5-s offsets were analyzed, and the event-level results reported in Figure 4 and Table 2 represent the medians across offsets

the resolution-specific signal-to-noise context (Anastasiou et al., 2022; Chojer et al., 2024):

$$T_{u,p}^{(\Delta,\phi)} = q_{0.99}\left(\left\{\left|z_j - z_{j-1}\right| : j \in Q\right\}\right) \quad (7)$$

where: T is the resolution-specific detection threshold, z is the degraded quiet-period series, j indexes consecutive quiet reports, and $q_{0.99}$ is the empirical 99th percentile.

For degraded event data, the operational baseline was the most recent report ending before the event for block means, or the most recent sample before the event for instantaneous sampling. An event was detected when its largest absolute deviation from that operational baseline exceeded T. Only events detected at native resolution by both co-located units were included in the pollutant-specific missed-event denominator. The 95th-percentile threshold was prespecified as a sensitivity analysis. This design avoids applying native high-frequency noise to coarse data and avoids selecting a detection rule after inspecting event outcomes, consistent with application-matched sensor evaluation (Anastasiou et al., 2022; Chojer et al., 2024).

Event-ranking stability and twin confirmation

For phase-sensitivity diagnostics, eligible events were ranked separately for each pollutant, interval, protocol, phase, and unit by baseline-relative peak magnitude. Inferential ranking statistics were constructed only after these deterministic transformations had been reduced within event. Specifically, degraded peak magnitude was summarized by the median across all phase offsets for each event and unit; the two technical units were then combined by their within-event median for Kendall's tau against the correspondingly combined native peak. The units remained separate only for the prespecified confirmation rule for pairwise reversals. A reversal between events a and b was twin-confirmed when (i) both units agreed on the native ordering, (ii) neither native unit had a tie, and (iii) both units agreed on the opposite ordering using their phase-median degraded peaks. The reversal fraction used the number of such pairs over the number of event pairs with native agreement. A phase-specific top-event change required both units to identify the same native top event and both to identify the same different degraded top event. These top-event results were reported as descriptive counts of deterministic offsets, such as 60/60, rather than as inferential proportions. Replicate-sensor disagreement has been used independently as an operational quality and degradation signal (deSouza et al., 2023; Manu & Rysanek, 2024).

Uncertainty, sensitivity, and external instrument check

The documented event was the inferential unit. For each pollutant, protocol, and interval, 95% uncertainty intervals were obtained from 2.000 bootstrap resamples of events with replacement using fixed seed 20260719. Peak retention, AUC retention, and detection were first reduced across phase within event and unit and then across the two units within event. For ranking outcomes, each bootstrap draw resampled complete event rows and recomputed Kendall's tau, the set of native-consistent pairs, and the twin-confirmed reversal fraction; neither phase offsets nor event pairs were sampled as independent observations. When every event-bootstrap draw produced the same boundary value, the point estimate was retained, and its population interval was marked not estimable rather than reported as a zero-width confidence interval. Top-event phase counts received no confidence interval. The event-bootstrap intervals describe heterogeneity across the observed event set; they do not imply random sampling of all possible dwellings or activities, a limitation that is especially important for event-resolved indoor datasets (Lovrić et al., 2025; Lunderberg et al., 2023).

Robustness checks included the alternative 95th-percentile detection rule; instantaneous sampling versus block averaging; the two co-located units; non-parametric width scaling; and comparison of event-peak ranks with the EDIAQI reference device at a common 1-min block mean. Spearman and Kendall rank correlations were used for that external check because the primary question concerns relative event priority, not absolute calibration; co-location literature likewise distinguishes relative agreement from calibration validity (deSouza et al., 2023; Levy Zamora et al., 2023).

The full workflow was implemented in Python 3.12 using pandas, NumPy, SciPy, Matplotlib, and seaborn. The script writes all processed datasets, phase-level results, tables, figures, checksums, and a machine-readable manifest. No manual result was inserted into the analytical tables, supporting the traceable sensor-network workflow recommended in current methodological guidance and open high-resolution monitoring studies (Diez et al., 2024; Zimmerman, 2022).

RESULTS

Native data quality and twin behavior

Provider 4 supplied essentially continuous 5-s data across the included period. The 488 grid rows with at least one missing selected value represented 0.14% of the 343,336-row grid. The two units showed strong agreement in native event ranking despite differences in absolute amplitude. Spearman correlations of native event peaks were 0.979 for $PM_{2.5}$, 0.973 for CO_2, and 0.979 for TVOC response. Pairwise native-order agreement was 96.0%, 95.1%, and 96.0%, respectively, establishing disagreement floors of 4.0–4.9% before any degradation (Figure 3; Supplementary Tables S1 and S3). This separation of relative agreement from absolute calibration follows current replicate-sensor evaluation practice (deSouza et al., 2023; Manu and Rysanek, 2024).

The two units agreed on the top native event for every response. The largest native $PM_{2.5}$ peak occurred during "Diffuser with Oil inside"; the largest CO_2 peak occurred during "Exercise Rowing with opened door to the Garden"; and the largest TVOC response occurred during "Gas Burner working with opened door." These identities are event rankings within the monitored room, not causal source factors or emission rates (Supplementary Table S4), a distinction required because event logs do not by themselves isolate source contributions (Bousiotis et al., 2023; Rathbone et al., 2025).

Peak attenuation and AUC preservation

Peak attenuation was strongly response- and protocol-dependent (Figure 4; Table 2). Under block averaging, the median retained $PM_{2.5}$ peak fell to 0.933 at 30 s, 0.872 at 1 min, 0.771 at 5 min, 0.728 at 10 min, and 0.619 at 30 min. CO_2 was less sensitive: retention was 0.997 at 1 min, 0.987 at 5 min, 0.976 at 10 min, and 0.930 at 30 min. TVOC response retained 0.993 at 1 min, 0.982 at 5 min, 0.965 at 10 min, and 0.882 at 30 min. The broad $PM_{2.5}$ bootstrap intervals reflect heterogeneity in event shape and duration rather than phase offsets being treated as additional sample size; comparable work also reports averaging-time dependence and strong source-to-source variation (Bulot et al., 2023; Jones et al., 2024).

Net-excursion AUC behaved differently from the peak (Figure 5; Table 2). At 5-min block averaging, median AUC retention was 0.998 for $PM_{2.5}$, 1.001 for CO_2, and 0.998 for TVOC response. At 10 min it remained 0.981, 0.985, and 0.990, respectively. At 30 min, boundary mixing and coarse representation became substantial and median retention declined to 0.864 for $PM_{2.5}$, 0.905 for CO_2, and 0.905 for TVOC response. The contrast between near-preserved AUC and attenuated peaks at 5 min demonstrates that a reporting interval can support integrated event burden while failing to represent short maxima (Bulot et al., 2023; Frischmon et al., 2025).

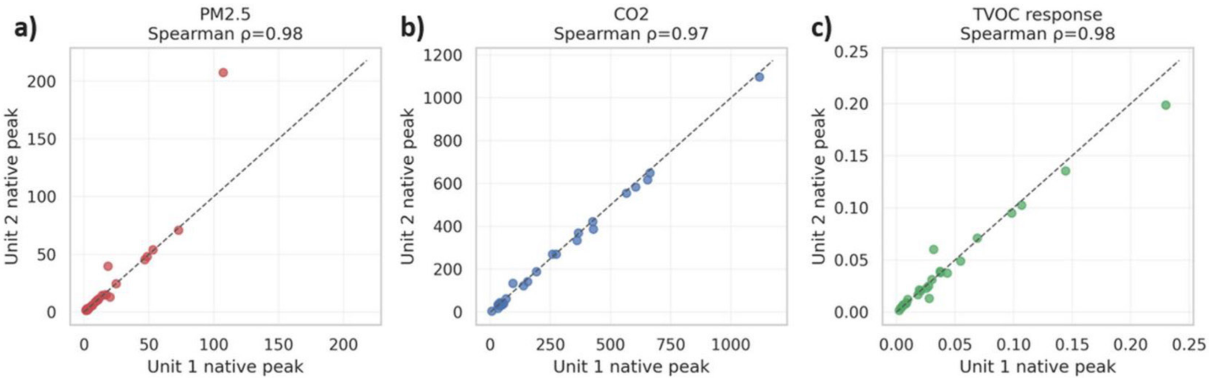

Figure 3. Agreement in native event-peak magnitudes between the two Provider 4 units for: a) $PM_{2.5}$, b) CO_2, and c) TVOC response. Each point represents one documented event. Dashed lines indicate the 1:1 equality line. Spearman's ρ values show strong monotonic agreement between the units, although differences in absolute peak magnitude were observed, particularly for $PM_{2.5}$

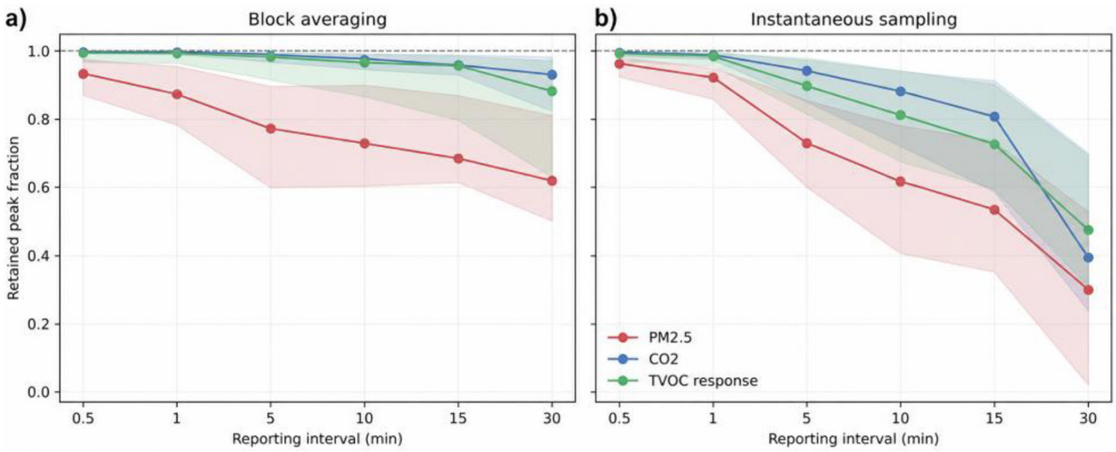

Figure 4. Retained event-peak fraction as a function of reporting interval for: a) block averaging and b) instantaneous sampling. Points represent event-level medians after aggregation across phase offsets and paired-unit results; shaded bands indicate 95% event-level bootstrap confidence intervals based on 2,000 resamples. Fractions were calculated relative to the native approximately 5-s peak. The horizontal dashed line indicates complete peak retention (fraction = 1)

Table 2. Core block-mean outcomes at decision-relevant reporting intervals

Response	Interval (min)	Peak retention	Net-AUC retention	Missed probability
$PM_{2.5}$	5	0.771 (0.598–0.895)	0.998 (0.991–1.007)	0.218 (0.053–0.408)
CO_2	5	0.987 (0.967–0.996)	1.001 (0.992–1.011)	0.066 (0.006–0.159)
TVOC response	5	0.982 (0.914–0.992)	0.998 (0.997–1.001)	0.083 (0.012–0.176)
$PM_{2.5}$	10	0.728 (0.603–0.899)	0.981 (0.971–0.999)	0.434 (0.237–0.656)
CO_2	10	0.976 (0.944–0.991)	0.985 (0.966–1.014)	0.104 (0.031–0.187)
TVOC response	10	0.965 (0.865–0.990)	0.990 (0.980–0.999)	0.146 (0.037–0.285)
$PM_{2.5}$	30	0.619 (0.500–0.810)	0.864 (0.819–0.935)	0.734 (0.558–0.902)
CO_2	30	0.930 (0.825–0.981)	0.905 (0.853–1.010)	0.295 (0.172–0.433)
TVOC response	30	0.882 (0.630–0.967)	0.905 (0.859–0.983)	0.369 (0.225–0.514)

Note: Author's analysis of the versioned EDIAQI archive. CI = 95% event-bootstrap interval.

Instantaneous sampling was markedly more phase-sensitive. At 30 min, median retained peaks were 0.300 for $PM_{2.5}$, 0.394 for CO_2, and 0.475 for TVOC response. The corresponding absolute-excursion AUC retentions were approximately 0.667, 0.740, and 0.715. Block means therefore dominated instantaneous samples for reconstructing both peak and cumulative event behavior at coarse intervals, although neither preserved native peak information (Figures 4 and 5; Table 2), consistent with the dependence of apparent performance on reporting protocol and averaging time (Bean, 2021; Bulot et al., 2023).

Missed events

At the native 99th-percentile detection rule, both units detected 19 $PM_{2.5}$ events and all 26 CO_2 and TVOC-response events. The denominator difference is important: missed probabilities describe only events with a reproducible native signal for that pollutant (Figure 6; Table 2), consistent with application-specific rather than device-generic detection assessment (Anastasiou et al., 2022; Chojer et al., 2024).

For 5-min block means, mean missed-event probability was 0.218 for $PM_{2.5}$, 0.066 for CO_2, and 0.083 for TVOC response. At 10 min, these probabilities increased to 0.434, 0.104, and 0.146. At 30 min they reached 0.734, 0.295, and 0.369. $PM_{2.5}$ detection did not improve monotonically between 30 s and 5 min because both the event excursion and the resolution-specific quiet threshold changed with averaging. This behavior supports recomputing the threshold at each resolution instead of assuming a fixed native noise level (Figure 6; Table

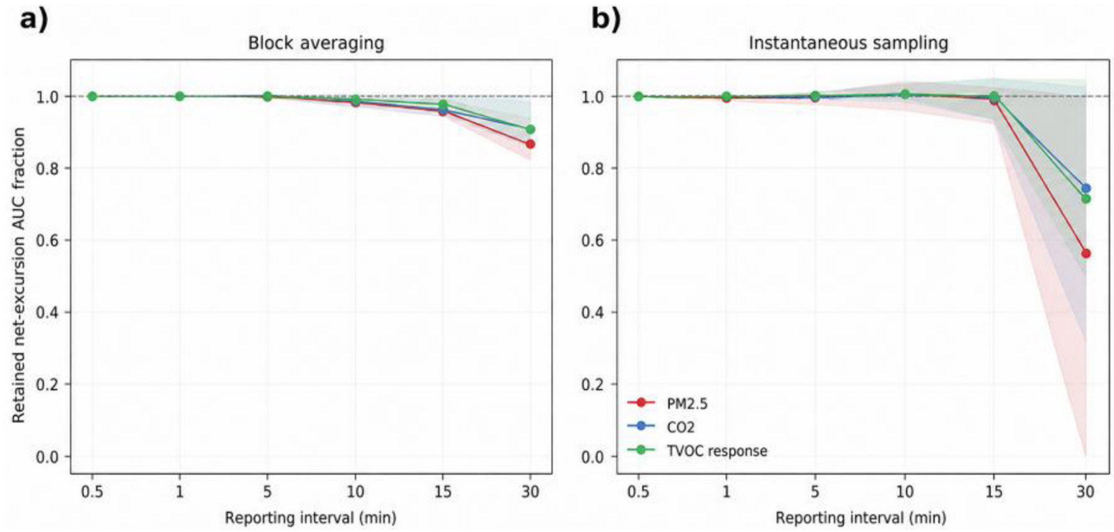

Figure 5. Retained net-excursion AUC fraction as a function of reporting interval for: a) block averaging and b) instantaneous sampling. The horizontal dashed line indicates complete retention (fraction = 1). Values above 1 may occur when a coarse reporting interval incorporates an adjacent excursion across the documented event boundary or when the signed native AUC is close to zero

2), because averaging changes both precision and transient response (Bean, 2021; Bulot et al., 2023).

The 95th-percentile sensitivity rule reduced missed-event probabilities for CO_2 and TVOC response and changed the exact $PM_{2.5}$ values, but it did not alter the qualitative conclusion that $PM_{2.5}$ events were most vulnerable and coarse instantaneous sampling was least reliable. Detection results should be interpreted as an operational signal-to-noise assessment, not as a health-based exceedance test (Figure 6; analysis workbook, sensitivity sheets), in line with guidance that validation criteria must match the intended application (Anastasiou et al., 2022; Chojer et al., 2024).

Event-ranking reversals

Event ranks remained highly stable at 30 s and 1 min block averaging. At 1 min, event-level Kendall tau was 0.953 for $PM_{2.5}$, 0.994 for CO_2, and 0.951 for TVOC response after phase and unit reduction. Twin-confirmed phase-median pairwise reversal fractions were 0.006, 0, and 0, respectively, all below their native unit-disagreement floors. The bootstrap interval was not estimable for the two observed zero fractions because all event resamples remained at the empirical boundary (Figure 7; Table 3). Treating replicate disagreement as a measured floor is supported by paired-sensor evaluation studies (deSouza et al., 2023; Manu and Rysanek, 2024).

At 5 min, event-level Kendall tau was 0.883 (95% event-bootstrap interval: 0.764–0.975) for $PM_{2.5}$, 0.951 (0.864–1.000) for CO_2, and 0.908 (0.794–0.994) for TVOC response. Twin-confirmed phase-median pairwise reversal fractions were 2.42% (0–6.37%), 0.97% (0–3.66%), and 2.88% (0–7.77%), respectively. Most importantly, the top $PM_{2.5}$ event changed in both co-located units for 60/60 phase offsets: “Diffuser with Oil inside,” which had the largest native peak, was replaced by “Exercise Rowing with opened door to the Garden.” This is a deterministic sensitivity result, not 60 independent replications, but it shows that the observed top-event change was not attributable to one clock alignment or disagreement between the twin units. CO_2 and TVOC top-event identities remained unchanged at 0/60 offsets and under block averaging through 30 min, although lower-ranked pairs increasingly reversed (Figure 7; Table 3; Supplementary Table S4). This finding is operationally relevant because short indoor $PM_{2.5}$ events can be spatially and temporally concentrated (Jones et al., 2024; Rathbone et al., 2025).

At 30-min block means, Kendall tau was 0.754 for $PM_{2.5}$, 0.729 for CO_2, and 0.840 for TVOC response, with twin-confirmed phase-median reversal fractions of 7.88%, 10.36%, and 4.81%, respectively. Their event-bootstrap intervals were broad: 0.553–0.911, 0.488–0.897, and 0.691–0.962 for tau, and 1.90–16.35%, 3.22–21.09%, and 0–12.59% for reversal fractions. Under 30-min instantaneous sampling, the corresponding tau estimates were

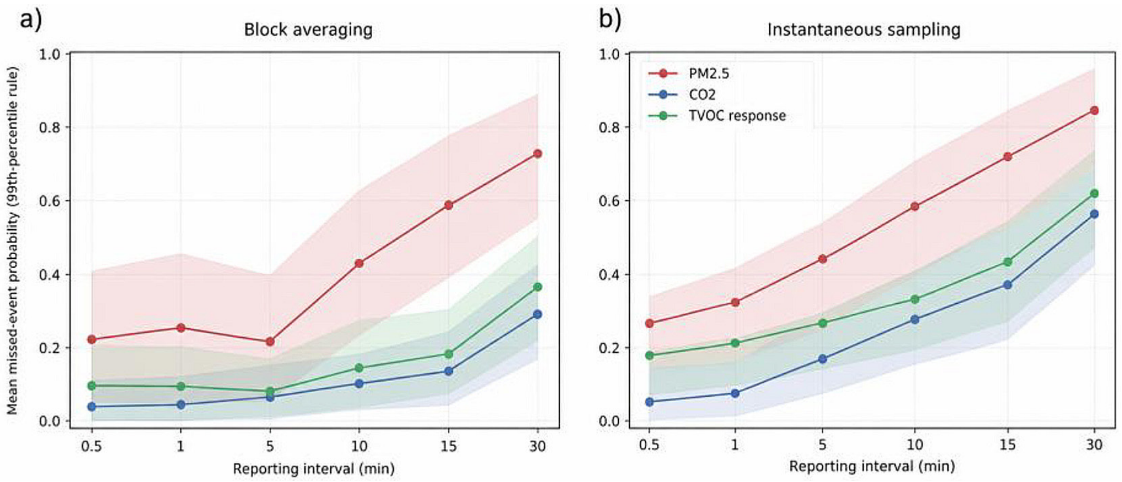

Figure 6. Mean missed-event probability as a function of reporting interval for: a) block averaging and b) instantaneous sampling, based on the resolution-specific 99th-percentile quiet-change rule. Denominators include only documented events detected at native resolution by both co-located units. Points represent mean missed-event probabilities, and shaded bands indicate 95% event-level bootstrap confidence intervals

0.292, 0.674, and 0.617, while reversal fractions were 31.52%, 11.97%, and 14.10%. Thus, reporting mechanism affected event prioritization in addition to reporting interval (Figure 7; Table 3), extending prior evidence that performance metrics depend on averaging and reporting choices (Bean, 2021; Bulot et al., 2023).

Characteristic-time scaling and reference-device check

Of 156 event–pollutant–unit native combinations, 61 had complete baseline-corrected half-height widths, 81 were right-censored, and 14 were left-censored. Complete widths represented 19 unique events. Peak retention generally decreased as Δ/w increased, but the empirical cloud did not collapse to a single curve. Values above one occurred principally where coarse blocks crossed event boundaries or where complex multi-peak structure violated the isolated-pulse approximation (Figure 8; phase-level scaling dataset); complex source, mixing, and persistence patterns are also reported in event-resolved indoor studies (Jones et al., 2024; Lunderberg et al., 2023).

Only 22 combinations, representing seven unique events, met the prespecified exponential-decay criteria. For a pure exponential decay averaged over a block beginning at the peak, the expected retained fraction is:

$$A\left(\frac{\Delta}{\tau_e}\right) = \frac{\tau_e}{\Delta}\left(1 - e^{-\frac{\Delta}{\tau_e}}\right) = \frac{1 - e^{-r}}{r}, \quad r = \Delta/\tau_e \tag{8}$$

where: A is the theoretically retained block-mean peak for a pure exponential decay, τ_e is the fitted decay time, Δ is the block interval, and $r = \Delta/\tau_e$ is the dimensionless interval.

Eligible observations were broadly consistent with declining retention as Δ/τ_e increased, but the subset was too small and selective to justify a universal fitted threshold. The theoretical curve is therefore a physical reference, not an estimated law for the room. The more inclusive width scaling remains the primary transfer-oriented result (Figure 8), consistent with cautions against transferring a single average-fit rule across sensors, sources, and environments (Bulot et al., 2023; Frischmon et al., 2025).

At a common 1-min block mean, Provider 4 event-peak rankings agreed well with the EDI-AQI reference device. $PM_{2.5}$ Spearman correlations were 0.905 for unit 1 and 0.880 for unit 2; corresponding Kendall correlations were 0.754 and 0.711. CO_2 Spearman correlations were 0.845 and 0.847, with Kendall correlations of 0.729 and 0.742. This check does not calibrate Provider 4, but it supports the use of relative event ranking as the principal outcome (Supplementary Table S2), consistent with the

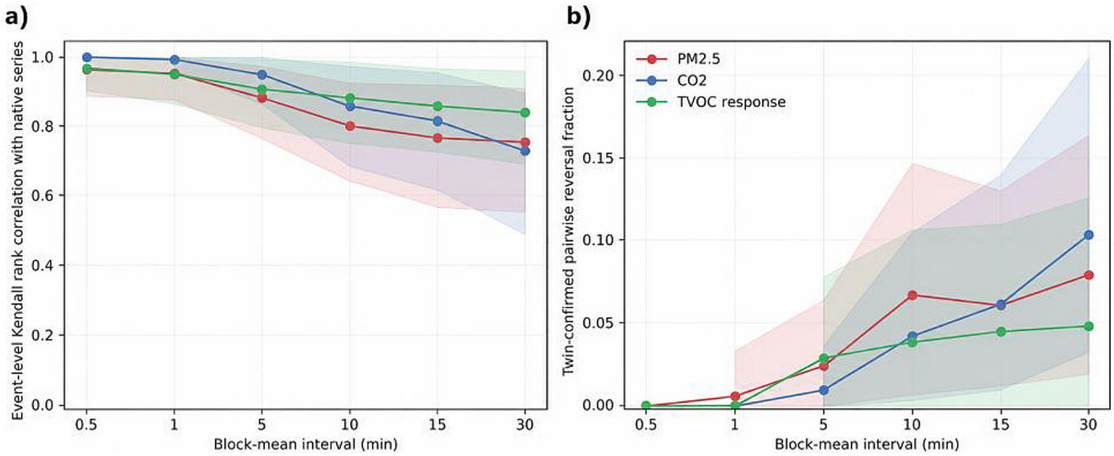

Figure 7. Stability of block-mean event rankings after phase offsets were reduced within each event and unit: a) Kendall correlation between degraded and native event-peak ranks and b) fraction of event pairs whose reversal was independently confirmed by both co-located units. Lines represent $PM_{2.5}$, CO_2, and TVOC response. Shaded bands are 95% event-bootstrap intervals; phase offsets and event pairs were not resampled as independent observations

Table 3. Block-mean event-ranking stability and twin-confirmed reversals

Response	Interval (min)	Events (n)	Kendall τ	Pair reversal fraction	Top-change offsets
$PM_{2.5}$	5	19	0.883 (0.764–0.975)	0.024 (0.000–0.064)	60/60
CO_2	5	26	0.951 (0.864–1.000)	0.010 (0.000–0.037)	0/60
TVOC response	5	26	0.908 (0.794–0.994)	0.029 (0.000–0.078)	0/60
$PM_{2.5}$	30	19	0.754 (0.553–0.911)	0.079 (0.019–0.164)	357/360
CO_2	30	26	0.729 (0.488–0.897)	0.104 (0.032–0.211)	0/360
TVOC response	30	26	0.840 (0.691–0.962)	0.048 (0.000–0.126)	0/360

Note: Point estimates reduce all phase offsets within event and unit before ranking. Parentheses are 95% percentile intervals from 2,000 event-cluster bootstrap resamples in which Kendall τ and the reversal denominator were recomputed. Top-change offsets are descriptive deterministic counts, not independent samples. NE = interval not estimable at an empirical boundary.

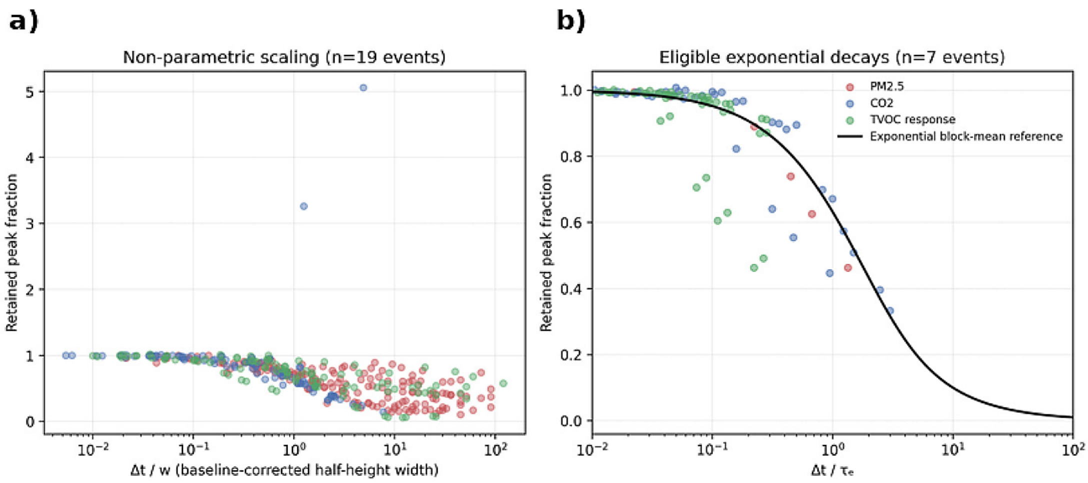

Figure 8. Dimensionless scaling of retained peak fraction: a) non-parametric scaling of the reporting interval, Δt, by the baseline-corrected half-height width, w, for events with complete width estimates; and b) scaling for the subset of eligible exponential-decay events, with Δt normalized by the estimated decay constant, τ_e. Points represent event-level observations for $PM_{2.5}$, CO_2, and TVOC response. The black curve represents the analytical block-mean response expected for an exponential decay and was not fitted to the observed data

distinction between monotonic agreement and concentration calibration (deSouza et al., 2023; Levy Zamora et al., 2023).

DISCUSSION

Principal finding: Resolution is an inference requirement

The central result is not simply that averaging lowers peaks. It is that the same five-minute block mean produced two different conclusions from the same native event record: integrated net AUC was almost unchanged, while the $PM_{2.5}$ peak was reduced by about 23% at the median and the identity of the highest-peak event reversed in both co-located units for every phase offset. A monitoring program designed for integrated burden could therefore accept an interval that would be unsuitable for peak-triggered alarms or event prioritization. Temporal resolution is consequently part of the measurement objective, not an interchangeable storage parameter (Bean, 2021; Frischmon et al., 2025).

This interpretation is consistent with indoor studies showing sharp, activity-dependent particle excursions (Jones et al., 2024; Rathbone et al., 2025) and large residential datasets that identify episodic indoor emissions as a distinct temporal component (Lunderberg et al., 2023; Wallace and Zhao, 2023). It is also consistent with evaluations demonstrating that sensor performance depends on source, environment, processing, and averaging choice (Bean, 2021; Bulot et al., 2023). The present design adds a controlled counterfactual: the high-resolution series and its degraded versions come from the same physical unit. The observed losses cannot be explained by comparing a fast sensor from one provider with a slower sensor from another (Levy Zamora et al., 2023; Manu and Rysanek, 2024).

Why $PM_{2.5}$ was most sensitive

$PM_{2.5}$ produced the strongest peak attenuation, missed-event probability, and top-event instability. This is physically plausible because short particle bursts can have rapid rise times and can be concentrated within a small part of a longer reporting block. Residential monitoring has repeatedly attributed high short-term $PM_{2.5}$ excursions to cooking, combustion, cleaning, and other occupant activities (Jones et al., 2024; Rathbone et al., 2025). Optical sensors also respond to aerosol size distribution, refractive index, humidity, sampled particle number, season, and calibration choice, which can change across sources and averaging times (Srishti S et al., 2023; Suriano and Prato, 2023). For that reason, this study does not interpret the absolute amplitude difference between the two Provider 4 units as a concentration-validation result. It relies instead on their strong agreement in event order and requires both to confirm a reversal (deSouza et al., 2023; Manu and Rysanek, 2024).

The oil-diffuser event is an instructive example. It was the top native $PM_{2.5}$ event in both units but contained a sharper high-amplitude excursion than the more sustained exercise/open-door episode. Five-minute averaging suppressed the short maximum enough to change the top event for all phase offsets. This mechanism accords with evidence that short indoor particle episodes and high-percentile sensor peaks are especially vulnerable to smoothing or underprediction (Frischmon et al., 2025; Jones et al., 2024). If a mitigation program used coarse data to select the “dominant source,” it would prioritize a different intervention. Because the competing event included exercise and an open door, “event-ranking reversal” is more accurate than “source-ranking reversal”; event logs and low-cost sensor signals do not by themselves isolate causal emission factors (Bousiotis et al., 2023; Rathbone et al., 2025).

CO_2 and TVOC-response regimes

CO_2 retained peaks and ranking more effectively than $PM_{2.5}$, consistent with a more sustained response during occupancy, exercise, and combustion-related events and with co-location studies reporting comparatively stable CO_2 channels (Afroz et al., 2023; Manu and Rysanek, 2024). In this dataset, five-minute block means retained a median of 98.7% of the native CO_2 peak and maintained Kendall tau above 0.90. Nevertheless, a 30-min interval missed nearly 30% of natively detectable CO_2 events on average and generated approximately 10.4% twin-confirmed pairwise reversals. Even a comparatively slow indoor response is not immune to coarse reporting when the objective is event detection or rank ordering (Ródenas García et al., 2022; Zheng et al., 2022).

The TVOC channel must be interpreted more cautiously. Its median peak retention resembled CO_2 at short intervals, but this does not establish that room VOC dynamics were intrinsically slow.

Metal-oxide TVOC channels can have device-dependent response and recovery, internal baseline processing, humidity sensitivity, and broad cross-sensitivity (Isaac et al., 2022; Papale et al., 2023). Large indoor co-location studies have likewise found substantially greater uncertainty for TVOC than for CO_2 channels (Demanega et al., 2021; Manu & Rysanek, 2024). The measured time scale is therefore a convolution of environmental dynamics and instrument response. This is why the manuscript uses "TVOC response" and why no chemically specific concentration or exposure conclusion is drawn (Baldelli, 2021; Papale et al., 2023).

Block means versus instantaneous reporting

At every coarse interval, instantaneous sampling was more phase-sensitive than block averaging. A momentary sample can miss a short event entirely, while a block mean contains some information whenever the event overlaps the block. The benefit of block averaging does not mean that its peak is unbiased: the block value is an integral divided by interval length and is therefore expected to attenuate short maxima. Rather, block means are the preferable reporting mechanism when data-rate constraints preclude native storage and cumulative event burden is important (Bean, 2021; Chacón-Mateos et al., 2025).

The all-phase design is central to this conclusion. A single arbitrary alignment could make instantaneous sampling appear unusually good or bad. By evaluating every possible 5-s phase, the analysis describes the full range of outcomes permitted by the specified interval. Phase offsets were then reduced within event, avoiding the false sample-size inflation that would result from treating hundreds of deterministic re-samplings as independent observations. This extends prior aggregation studies by treating alignment as a design variable rather than fixing one reporting clock (Bean, 2021; Bulot et al., 2023).

Practical design implications

The empirical limits differ by outcome. For block means in this dataset, CO_2 met three relatively strict point-estimate criteria – median peak retention at least 0.90, missed-event probability at most 0.10, and Kendall tau at least 0.90 – through 5 min. TVOC response also met the peak, detection, and point-estimate ranking criteria through 5 min, although the lower event-bootstrap limit for tau at that interval was 0.794; a 1-min interval is therefore more conservative when ranking uncertainty matters. $PM_{2.5}$ retained at least 90% of the median peak only at 30 s; its Kendall correlation remained above 0.90 through 1 min, but no tested degraded interval achieved a mean missed-event probability below 0.10 under the conservative 99th-percentile rule. These are not universal standards; they are transparent decision thresholds applied to this event set, consistent with objective-specific rather than device-generic sampling design (Bean, 2021; Bulot et al., 2023) (Table 4).

For an indoor network whose principal output is integrated event burden, 5-min block means were adequate for all three responses in the present room, and 10-min block means still retained at least 98% of the median net AUC. For short-term alarms, peak compliance, or $PM_{2.5}$ event prioritization, native or sub-minute storage is preferable. A pragmatic architecture is to calculate and transmit routine block means while retaining high-frequency data locally around triggers, an approach compatible with sensor-network guidance that balances information content, power, and data handling (Barros et al., 2023; Zimmerman, 2022). The validity of such a trigger would need to be tested against the specific device noise, event duration, and health or operational threshold (Bean, 2021; Ródenas García et al., 2022).

Characteristic-time scaling offers a route to transfer beyond clock minutes. The trend with Δ/w supports the intuitive rule that the reporting interval should be small relative to event width.

Table 4. Empirical upper reporting intervals by monitoring objective in the analyzed event set

Response	Peak ≥0.90	Missed ≤0.10	Kendall τ ≥0.90	Conservative interpretation
$PM_{2.5}$	30 s	None tested	1 min	≤30 s for peaks; native/sub-minute for conservative detection
CO_2	30 min	5 min	5 min	5-min block mean
TVOC response	15 min	5 min	5 min	5-min point estimate; use 1 min when ranking uncertainty is consequential

Note: Empirical thresholds for this event set; they are design implications, not universal standards.

However, the incomplete collapse and widespread censoring show why a single universal coefficient should not be claimed from these data. Complex indoor episodes include continued generation, ventilation, overlapping events, deposition, mixing, and sensor response, as event-resolved indoor datasets and aerosol-persistence studies also demonstrate (Jones et al., 2024; Lunderberg et al., 2023). The exponential block-mean curve is useful as a theoretical lower-complexity benchmark, but only seven events met the strict decay criteria; peak-oriented sensor work similarly cautions against relying on global average-fit statistics alone (Bulot et al., 2023; Frischmon et al., 2025).

Strengths, limitations, and reproducibility

The strongest feature is ground truth by construction for the degradation question. Native observations, event timestamps, degraded observations, and the error relative to native are all observable. The design uses one provider for the primary comparison, all sampling phases as deterministic sensitivity transformations, event-cluster bootstrap uncertainty after within-event reduction, two co-located units as a measured noise floor, resolution-specific detection thresholds, and an external rank check against the reference device. These choices align with contemporary recommendations for co-location, replicate-device QA, and transparent sensor-network evaluation (Levy Zamora et al., 2023; Manu and Rysanek, 2024). The analysis is fully reproducible from the open, versioned EDIAQI archive (Lovrić et al., 2025), following the same general principle of pairing high-resolution sensor data with explicit provenance and validation artifacts (Bulot et al., 2023; Fissore et al., 2024).

Several limitations bound the inference. First, the events occurred in one monitored experimental room in Croatia. Numerical intervals cannot be generalized to other buildings without considering room volume, ventilation, source duration, mixing, background, and sensor response (Glenn et al., 2023; Lovrić et al., 2025). Second, the native low-cost series is an operational temporal reference rather than a perfect physical concentration standard; the 1-min reference-device rank check is supportive but cannot validate 5-s peak amplitude (Bulot et al., 2023; Diez et al., 2024). Third, TVOC dynamics are instrument-specific, and $PM_{2.5}$ optical response may depend on event aerosol properties (Isaac et al., 2022; Papale et al., 2023). Fourth, event timestamps define analysis windows but do not isolate causal source contributions; some event blocks can contain residual or adjacent activity (Bousiotis et al., 2023; Rathbone et al., 2025). Fifth, only 19 $PM_{2.5}$ events were natively detected by both units under the conservative rule, widening uncertainty. Sixth, width estimates were censored for most event–response combinations and exponential fits were eligible for only seven events. Seventh, the repository's current event JSON yielded 34 occurrences while the Data Descriptor states 33 experiments, and the checked Provider 4 file had fewer rows than reported for an earlier distribution (Lovrić et al., 2025). The supplied event inventory, checksum, and exclusion table make those discrepancies auditable rather than silently reconciling them (Diez et al., 2024; Fissore et al., 2024).

These limitations favor a specific interpretation: the study demonstrates how reporting choices can alter event-level decisions in a well-documented indoor dataset. It does not estimate population exposure, health risk, universal source strength, or a universal sampling law; those uses require calibration and validation matched to the intended deployment environment (Anastasiou et al., 2022; Chojer et al., 2024).

CONCLUSIONS

Controlled temporal degradation of two co-located indoor sensor units reporting at approximately 5 s showed that both reporting interval and reporting mechanism materially affected event-oriented inferences. Five-minute block means nearly preserved the net event area under the curve, with median retention values of 0.998 for $PM_{2.5}$, 1.001 for CO_2, and 0.998 for the TVOC response, while the median $PM_{2.5}$ peak was reduced to 77.1% of its native value. At the same interval, the highest-peak $PM_{2.5}$ event changed identity in both units across all 60 phase offsets evaluated.

Missed-event probability and pairwise ranking reversals increased as reporting intervals became coarser. At 10 min, mean missed-event probability reached 0.434 for $PM_{2.5}$, 0.104 for CO_2, and 0.146 for the TVOC response. Instantaneous sampling was more phase-sensitive than block averaging; at 30 min, it retained median peak fractions of 0.300, 0.394, and 0.475, compared with 0.619, 0.930, and 0.882 under block averaging.

Within the monitored environment, temporal-resolution performance depended on the evaluated outcome. Five-minute CO_2 block means met the predefined criteria for peak retention, event detection, and ranking stability. For the TVOC response, the point-estimate ranking criterion was met through 5 min, but 1 min is the more conservative interval when the event-bootstrap uncertainty is considered; its peak-retention and detection criteria were met through 5 min. For $PM_{2.5}$, median peak retention of at least 90% occurred only at 30 s, and none of the evaluated degraded intervals met the conservative missed-event criterion. Overall, integrated event burden was more resistant to temporal degradation than transient peaks, event detection, and event prioritization.

The original EDIAQI data are available under CC BY 4.0 from Zenodo, version DOI 10.5281/zenodo.17151843 (concept DOI 10.5281/zenodo.14697453). The reproducibility package accompanying this manuscript contains the exact Provider 4 analytical extract, event inventory, quiet-period mask, all degradation results, thresholds, phase-level rank results, summary tables, figures, code, and checksums. The original unmodified source ZIP is included separately with attribution.

REFERENCES

1. Afroz, R., Guo, X., Cheng, C.-W., Delorme, A., Duruisseau-Kuntz, R., Zhao, R. (2023). Investigation of indoor air quality in university residences using low-cost sensors. *Environmental Science: Atmospheres*, *3*(2), 347–362. https://doi.org/10.1039/D2EA00149G
2. Anastasiou, E., Vilcassim, M. J. R., Adragna, J., Gill, E., Tovar, A., Thorpe, L. E., Gordon, T. (2022). Feasibility of low-cost particle sensor types in long-term indoor air pollution health studies after repeated calibration, 2019–2021. *Scientific Reports*, *12*(1), 14571. https://doi.org/10.1038/s41598-022-18200-0
3. Baldelli, A. (2021). Evaluation of a low-cost multichannel monitor for indoor air quality through a novel, low-cost, and reproducible platform. *Measurement: Sensors*, *17*, 100059. https://doi.org/10.1016/j.measen.2021.100059
4. Barros, N., Sobral, P., Moreira, R. S., Vargas, J., Fonseca, A., Abreu, I., Guerreiro, M. S. (2023). SchoolAIR: A citizen science IoT framework using low-cost sensing for indoor air quality management. *Sensors*, *24*(1), 148. https://doi.org/10.3390/s24010148
5. Bean, J. K. (2021). Evaluation methods for low-cost particulate matter sensors. *Atmospheric Measurement Techniques*, *14*(11), 7369–7379. https://doi.org/10.5194/amt-14-7369-2021
6. Bousiotis, D., Allison, G., Beddows, D. C. S., Harrison, R. M., Pope, F. D. (2023). Towards comprehensive air quality management using low-cost sensors for pollution source apportionment. *Npj Climate and Atmospheric Science*, *6*(1), 122. https://doi.org/10.1038/s41612-023-00424-0
7. Bulot, F. M. J., Ossont, S. J., Morris, A. K. R., Basford, P. J., Easton, N. H. C., Mitchell, H. L., Foster, G. L., Cox, S. J., Loxham, M. (2023). Characterisation and calibration of low-cost PM sensors at high temporal resolution to reference-grade performance. *Heliyon*, *9*(5), e15943. https://doi.org/10.1016/j.heliyon.2023.e15943
8. Byrne, R., Ryan, K., Venables, D. S., Wenger, J. C., Hellebust, S. (2023). Highly local sources and large spatial variations in $PM_{2.5}$ across a city: Evidence from a city-wide sensor network in Cork, Ireland. *Environmental Science: Atmospheres*, *3*(5), 919–930. https://doi.org/10.1039/D2EA00177B
9. Chacón-Mateos, M., García-Salamero, H., Laquai, B., Vogt, U. (2025). Calibration and performance evaluation of $PM_{2.5}$ and NO_2 air quality sensors for environmental epidemiology. *Atmospheric Measurement Techniques*, *18*(16), 4061–4085. https://doi.org/10.5194/amt-18-4061-2025
10. Chojer, H., Branco, P. T. B. S., Martins, F. G., Sousa, S. I. V. (2024). A novel low-cost sensors system for real-time multipollutant indoor air quality monitoring – Development and performance. *Building and Environment*, *266*, 112055. https://doi.org/10.1016/j.buildenv.2024.112055
11. Corona, J., Tondini, S., Gallichi Nottiani, D., Scilla, R., Gambaro, A., Pasut, W., Babich, F., Lollini, R. (2024). Environmental quality bOX (EQ-OX): A portable device embedding low-cost sensors tailored for comprehensive indoor environmental quality monitoring. *Sensors*, *24*(7), 2176. https://doi.org/10.3390/s24072176
12. Cowell, N., Chapman, L., Bloss, W., Srivastava, D., Bartington, S., Singh, A. (2023). Particulate matter in a lockdown home: Evaluation, calibration, results and health risk from an IoT enabled low-cost sensor network for residential air quality monitoring. *Environmental Science: Atmospheres*, *3*(1), 65–84. https://doi.org/10.1039/D2EA00124A
13. Demanega, I., Mujan, I., Singer, B. C., Anđelković, A. S., Babich, F., Licina, D. (2021). Performance assessment of low-cost environmental monitors and single sensors under variable indoor air quality and thermal conditions. *Building and Environment*, *187*, 107415. https://doi.org/10.1016/j.buildenv.2020.107415
14. deSouza, P., Barkjohn, K., Clements, A., Lee, J.,

Kahn, R., Crawford, B., Kinney, P. (2023). An analysis of degradation in low-cost particulate matter sensors. *Environmental Science: Atmospheres*, *3*(3), 521–536. https://doi.org/10.1039/D2EA00142J

15. Diez, S., Lacy, S., Coe, H., Urquiza, J., Priestman, M., Flynn, M., Marsden, N., Martin, N. A., Gillott, S., Bannan, T., Edwards, P. M. (2024). Long-term evaluation of commercial air quality sensors: An overview from the QUANT (Quantification of Utility of Atmospheric Network Technologies) study. *Atmospheric Measurement Techniques*, *17*(12), 3809–3827. https://doi.org/10.5194/amt-17-3809-2024
16. Ferro, A. R., Zíková, N., Masiol, M., Satsangi, G. P., Twomey, T., Chalupa, D. C., Rich, D. Q., Hopke, P. K. (2022). Residential indoor and outdoor PM measured using low-cost monitors during the heating season in monroe county, NY. *Aerosol and Air Quality Research*, *22*(9), 220210. https://doi.org/10.4209/aaqr.220210
17. Fissore, V. I., Arcamone, G., Astolfi, A., Barbaro, A., Carullo, A., Chiavassa, P., Clerico, M., Fantucci, S., Fiori, F., Gallione, D., Giusto, E., Lorenzati, A., Mastromatteo, N., Montrucchio, B., Pellegrino, A., Piccablotto, G., Puglisi, G. E., Ramirez-Espinosa, G., Raviola, E., … Shtrepi, L. (2024). Multi-sensor device for traceable monitoring of indoor environmental quality. *Sensors*, *24*(9), 2893. https://doi.org/10.3390/s24092893
18. Frischmon, C., Silberstein, J., Guth, A., Mattson, E., Porter, J., Hannigan, M. (2025). Improving the quantification of peak concentrations for air quality sensors via data weighting. *Atmospheric Measurement Techniques*, *18*(13), 3147–3159. https://doi.org/10.5194/amt-18-3147-2025
19. Giordano, M. R., Malings, C., Pandis, S. N., Presto, A. A., McNeill, V. F., Westervelt, D. M., Beekmann, M., Subramanian, R. (2021). From low-cost sensors to high-quality data: A summary of challenges and best practices for effectively calibrating low-cost particulate matter mass sensors. *Journal of Aerosol Science*, *158*, 105833. https://doi.org/10.1016/j.jaerosci.2021.105833
20. Glenn, K., He, J., Rochlin, R., Teng, S., Hecker, J. G., Novosselov, I. (2023). Assessment of aerosol persistence in ICUs via low-cost sensor network and zonal models. *Scientific Reports*, *13*(1), 3992. https://doi.org/10.1038/s41598-023-30778-7
21. Ilacqua, V., Scharko, N., Zambrana, J., Malashock, D. (2022). Survey of residential indoor particulate matter measurements 1990–2019. *Indoor Air*, *32*(7). https://doi.org/10.1111/ina.13057
22. Isaac, N. A., Pikaar, I., Biskos, G. (2022). Metal oxide semiconducting nanomaterials for air quality gas sensors: Operating principles, performance, and synthesis techniques. *Microchimica Acta*, *189*(5), 196. https://doi.org/10.1007/s00604-022-05254-0
23. Jones, H., Kumar, A., O'Leary, C., Dillon, T., Rolfo, S. (2024). Experimental and computational investigation of the emission and dispersion of fine particulate matter (PM2.5) during domestic cooking. *Atmosphere*, *15*(12), 1517. https://doi.org/10.3390/atmos15121517
24. Levy Zamora, M., Buehler, C., Datta, A., Gentner, D. R., Koehler, K. (2023). Identifying optimal co-location calibration periods for low-cost sensors. *Atmospheric Measurement Techniques*, *16*(1), 169–179. https://doi.org/10.5194/amt-16-169-2023
25. Lovrić, M., Petrić, V., Strbad, D., Terzić, T., Frka, S., Kušan, A. C., Fermoso, J., Düsing, S., Alas, H. D., Ladavac, M. D., Bilić, I., Batrac, M., Kecorius, S., Pehnec, G., Horvat, T., Jakovljević, I., Račić, N., Bešlić, I., Brzoja, D., … Mureddu, F. (2025). Indoor and ambient air pollution dataset using a multi-instrument approach and total event monitoring. *Scientific Data*, *12*(1), 1584. https://doi.org/10.1038/s41597-025-05847-3
26. Lunderberg, D. M., Liang, Y., Singer, B. C., Apte, J. S., Nazaroff, W. W., Goldstein, A. H. (2023). Assessing residential $PM_{2.5}$ concentrations and infiltration factors with high spatiotemporal resolution using crowdsourced sensors. *Proceedings of the National Academy of Sciences*, *120*(50), e2308832120. https://doi.org/10.1073/pnas.2308832120
27. Manu, S., Rysanek, A. (2024). A co-location study of 87 low-cost environmental monitors: Assessing outliers, variability, and uncertainty. *Buildings*, *14*(9), 2965. https://doi.org/10.3390/buildings14092965
28. Mousavi, A., Wu, J. (2021). Indoor-generated $PM_{2.5}$ During COVID-19 shutdowns across California: application of the purpleair indoor–outdoor low-cost sensor network. *Environmental Science & Technology*, *55*(9), 5648–5656. https://doi.org/10.1021/acs.est.0c06937
29. Papale, L., Catini, A., Capuano, R., Allegra, V., Martinelli, E., Palmacci, M., Tranfo, G., Di Natale, C. (2023). Personal VOCs exposure with a sensor network based on low-cost gas sensor, and machine learning enabled indoor localization. *Sensors*, *23*(5), 2457. https://doi.org/10.3390/s23052457
30. Rathbone, C. J., Bousiotis, D., Rose, O. G., Pope, F. D. (2025). Using low-cost sensors to assess common air pollution sources across multiple residences. *Scientific Reports*, *15*(1), 1803. https://doi.org/10.1038/s41598-025-85985-1
31. Ródenas García, M., Spinazzé, A., Branco, P. T. B. S., Borghi, F., Villena, G., Cattaneo, A., Di Gilio, A., Mihucz, V. G., Gómez Álvarez, E., Lopes, S. I., Bergmans, B., Orłowski, C., Karatzas, K., Marques, G., Saffell, J., Sousa, S. I. V. (2022). Review of low-cost sensors for indoor air quality: Features and applications. *Applied Spectroscopy Reviews*, *57*(9–10), 747–779. https://doi.org/10.1080/05704928.2022.2085734
32. Sá, J. P., Alvim-Ferraz, M. C. M., Martins, F. G., Sousa, S. I. V. (2022). Application of the low-cost

sensing technology for indoor air quality monitoring: A review. *Environmental Technology & Innovation*, *28*, 102551. https://doi.org/10.1016/j.eti.2022.102551

33. Srishti S, -, Agrawal, P., Kulkarni, P., Gautam, H. C., Kushwaha, M., Sreekanth, V. (2023). Multiple PM low-cost sensors, multiple seasons' data, and multiple calibration models. *Aerosol and Air Quality Research*, *23*(3), 220428. https://doi.org/10.4209/aaqr.220428
34. Suriano, D., Prato, M. (2023). An investigation on the possible application areas of low-cost pm sensors for air quality monitoring. *Sensors*, *23*(8), 3976. https://doi.org/10.3390/s23083976
35. Tryner, J., Phillips, M., Quinn, C., Neymark, G., Wilson, A., Jathar, S. H., Carter, E., Volckens, J. (2021). Design and testing of a low-cost sensor and sampling platform for indoor air quality. *Building and Environment*, *206*, 108398. https://doi.org/10.1016/j.buildenv.2021.108398
36. Wall, D., McCullagh, P., Cleland, I., Bond, R. (2021). Development of an Internet of Things solution to monitor and analyse indoor air quality. *Internet of Things*, *14*, 100392. https://doi.org/10.1016/j.iot.2021.100392
37. Wallace, L., Zhao, T. (2023). Spatial variation of PM2.5 indoors and outdoors: Results from 261 regulatory monitors compared to 14,000 low-cost monitors in three western states over 4.7 years. *Sensors*, *23*(9), 4387. https://doi.org/10.3390/s23094387
38. Whitehill, A. R., Lunden, M., LaFranchi, B., Kaushik, S., Solomon, P. A. (2024). Mobile air quality monitoring and comparison to fixed monitoring sites for instrument performance assessment. *Atmospheric Measurement Techniques*, *17*(9), 2991–3009. https://doi.org/10.5194/amt-17-2991-2024
39. Zheng, H., Krishnan, V., Walker, S., Loomans, M., Zeiler, W. (2022). Laboratory evaluation of low-cost air quality monitors and single sensors for monitoring typical indoor emission events in Dutch daycare centers. *Environment International*, *166*, 107372. https://doi.org/10.1016/j.envint.2022.107372
40. Zimmerman, N. (2022). Tutorial: Guidelines for implementing low-cost sensor networks for aerosol monitoring. *Journal of Aerosol Science*, *159*, 105872. https://doi.org/10.1016/j.jaerosci.2021.105872